Electronic Supplementary Material (ESI) for Nanoscale.

Tunable Growth of High-Density ZIF Nanoshells on Gold Nanoparticles Isolated in an Optical Trap

Supplementary Information

Daniel Jackson[1], Maitreya Rose[2], Maria Kamenetska[1,2,3]
[1]Department of Chemistry, Boston University, Boston MA 02215.
[2]Department of Physics, Boston University, Boston MA 02215.
[3]Division of Material Science and Engineering; Boston University, Boston MA 02215.

Contents

Materials

Gold nanoparticles (80 nm, AuNPs) are obtained from Nanopartz (#AC11-80-CIT-DIH-100-1). Polyvinylpyrolidone (PVP)(#PVP40-50G), zinc nitrate hexahydrate (#228737-100G), 2-methylimidazole (2-Mim)(#M50850-100G), benzimidazole (Bim) (#194123-5G), 6-bromobenzimidazole (6-BBim)(#702188-1G), 4-tertbutylimidazole (4-TBim)(#CBR01595-1G), ethanol (#1117270500), dimethylformamide (DMF)(#D4551-250ML), and water (#W4502-1L) are obtained from Millipore Sigma. Glass slides (#260202) and coverslips (#260341) are obtained from Ted Pella.

Procedure

Preparation of precursor solution

Precursor solutions are prepared based on previous literature procedures.[1,2] For growth in ethanol—the condition primarily used in this manuscript—we prepared 25 mM $Zn(NO_3)_2{\cdot}6H_2O$ (0.0372 g, $1.25x10^{-4}$ mol) solution in 5 mL of ethanol, and 50 mM 2-Mim (0.0205 g, $2.5\ x10^{-4}$ mol) solution in 5 mL of ethanol. In water experiments, triethylamine was added to the 2-Mim precursor solution at a concentration of 0.25 M to help drive the reaction.[3]

Functionalizing AuNPs with PVP

AuNPs are coated with PVP by adapting a previously reported procedure.[1] Briefly, gold nanoparticles are dispersed in 19.5 mL of ethanol and 500 μL of a 25 mg/mL PVP solution is added to the mixture. The solution is left to stir under room temperature for 24 hours. This process replaces citrate stabilizer on the AuNPs with PVP molecules. Sample is centrifuged at 7500 rpm for 15 minutes, and then decanted. The following wash is then performed 3 times: (i) disperse AuNPs in 1 mL of ethanol; (ii) sonicate sample for 30 seconds and vortexe for 30 seconds, until no visible clumps remain; (iii) centrifuged7 minutes at 9000 rpm and remove supernatant; (iv) after final wash, disperse AuNPs in the desired solvent. Storing in water results in the longest shelf life, of at least 3 months. In other solvents (e.g. ethanol and DMF), we observe NPs sticking to the edge of the tube and non-dispersible clumps falling out of solution after a few weeks.

Combing gold and precursors

PVP AuNPs is dispersed in 100 mL of solvent and Zn^{2+} precursor solution is added and vortexed for 10 seconds to combine. The solution is left to sit for 5 minutes. PVP acts as a chelating agent and helps retain Zn^{2+} ions near the surface. Attempts to grow ZIF without PVP were unsuccessful. 2-Mim solution is added to mixture. The solution is vortexed for 10 seconds to combine mixture. Growth of ZIF nanoshells can be performed immediately after addition of 2-Mim.

Sample preparation

After the mixture is prepared, 50 μL of solution are injected into a sample chamber made up of a glass coverslip adhered to a glass slide with parafilm. Slide is placed in the optical tweezer instrument above an NA=1.45 oil immersion objective. Schematic of instrument shown in Figure 1A.

Measurements and Models

Growth of ZIF

Darkfield illumination is used to locate particles, which are then directed towards the trapping laser position by adjusting the nanopositioning stage position. Upon trapping, we begin collecting spectra at 100 ms acquisition per scan over the spectral range of 496.184 nm – 702.815 nm. Spectra are collected continuously until the particle becomes unstable in the trap and is ejected or 500 seconds has passed. We attribute the ejection to an increased scattering cross section due to growth of the crystal on the AuNP, resulting in an increased repulsive force from the trapping beam. This procedure can be repeated within the same sample cell for at least two hours. At longer times, we observe free floating ZIF crystals interfering with measurements. In the case of higher precursor concentrations (Figure S4), small ZIF crystals form in the background and interfered with experiments.

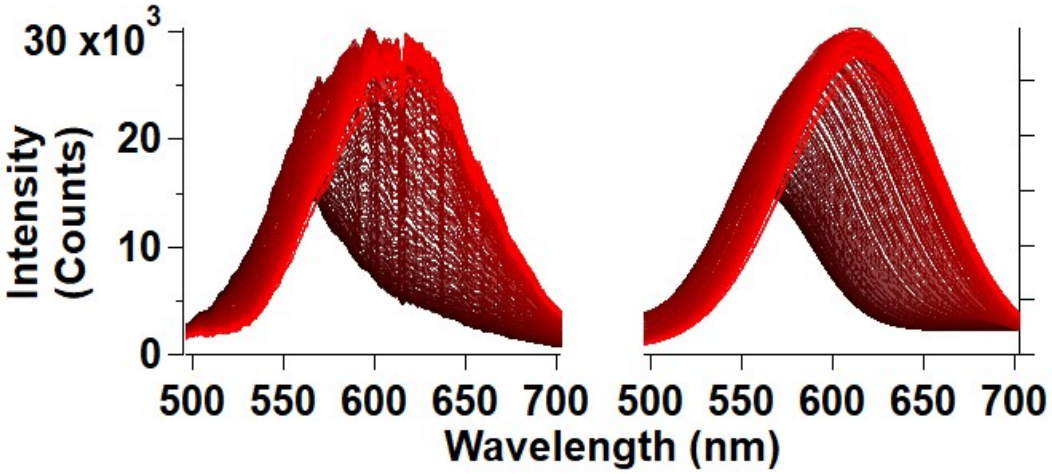

Figure S1: Plots of a full time sequence for the data presented in Figure 2A and 2C where dark curves represent the initial spectra and red represents the final spectra. Left is the raw data collected by the spectrometer, and the right is the Gaussian fits to those same lines.

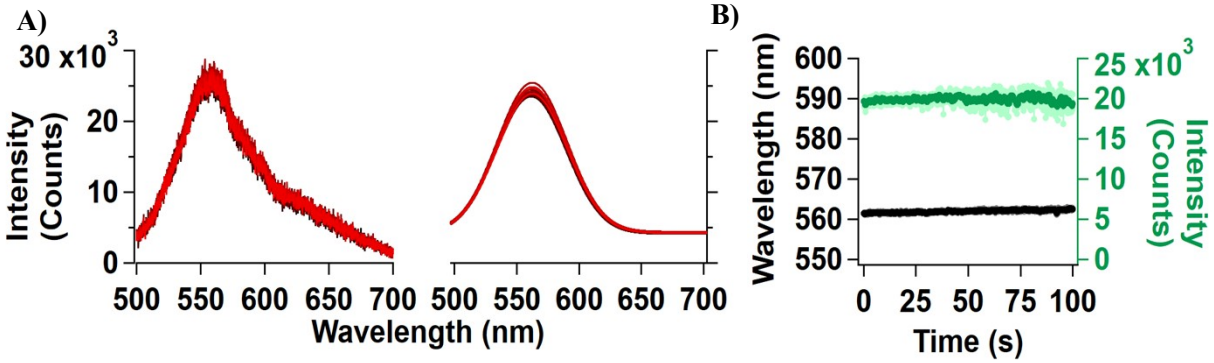

Figure S2: **A)** Control measurement DF spectra collected following heating of an optically trapped, 80 nm AuNP in the presence of in $Zn(NO_3)_2$ ethanol. **B)** Plot of the peak wavelengths (left, back) and associated intensities (right, green) against time.

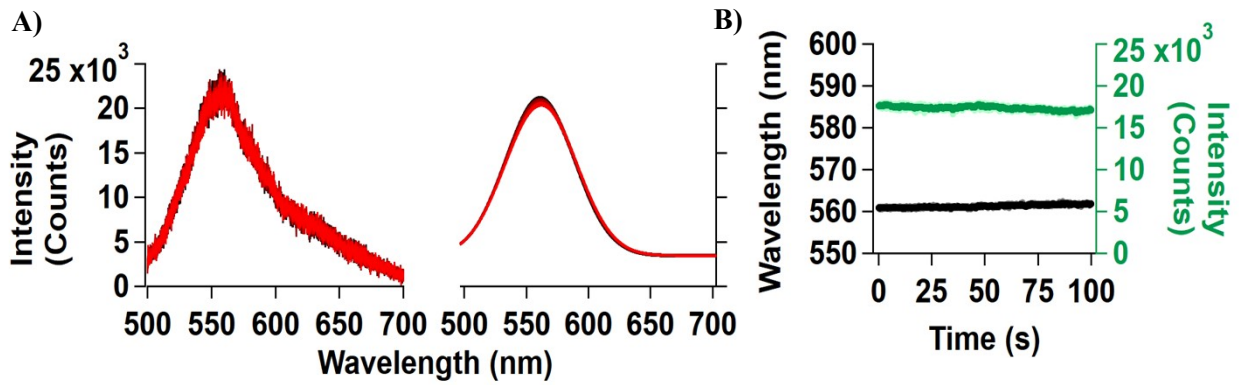

Figure S3: **A)** Control measurement DF spectra collected following heating of an optically trapped, 80 nm AuNP in the presence of 2-methylimidazole dispersed in ethanol. **B)** Plot of the peak wavelengths (left, back) and associated intensities (right, green) against time.

Choosing precursor concentrations

Figure S4 shows various concentration pairs of ZIF-8 precursors in the final mixture used to initiate growth. We determined that the optimal ratio of 2-Mim:Zn^{2+} in these experiments is approximately 3:1. The concentrations in the final mixture used throughout the main manuscript is 1 mM:0.33 mM (2-Mim:Zn^{2+}). Our 3:1 ratio agrees with a previously reported encapsulation procedure,[2] but differs from the 1:1 ratio found in procedures for bulk ZIF-8 crystal growth.[4] All other ZIF crystals were grown using the same 1 mM:0.33 mM concentration and ratio of imidazole derivative to metal ions. In water, there is also a concentration of ~10 mM TEA in the final reaction mixture as suggested by Khan et al.[3]

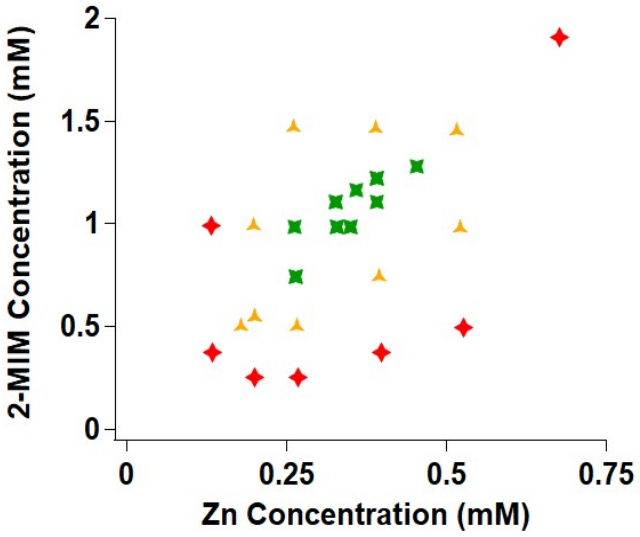

Figure S4: Plot of the Zn^{2+} and 2-MIM concentrations used in experiments. Found the best use concentration ratio of the two precursors to be 3:1, Mim:Zn. Green points represent concentrations that yielded steady and reproducible growth of ZIF-8 crystals on the surface of the gold. Yellow points represent concentrations that either resulted in growth that was restrictively slow or had small ZIF-8 crystals form in the solution background. Red represents concentrations where either no growth was observed, or an excessive amount of ZIF-8 crystals grew in the background.

Raman spectra collection

Raman spectra are collected while the ZIF crystal is growing on the AuNP surface. A particle is guided into the trap, followed by introducing the Raman excitation beam, which has been aligned to match the trap focal position. Raman measurement are performed using a 532 nm excitation beam, with a 1 min acquisition time, on a single, optically-trapped, 80 nm AuNP during crystal growth. A long exposure time is necessary because the Raman excitation power must be kept low (<50 mW before objective) so as not to destabilize trapped nanoparticle, and because only a quarter of the signal is reaching the spectrometer due to the presence of two 50/50 splitters. Long-pass Raman line filter is used to filter out the excitation beam (Semrock part #BLP01-532R-25). This filter prevents detection of signal below 540 nm (~400 cm^{-1} shift from excitation). Zn-N stretches are expected to be between 150 – 300 cm^{-1}, so we are unable to detect them in the current system.[5,6]

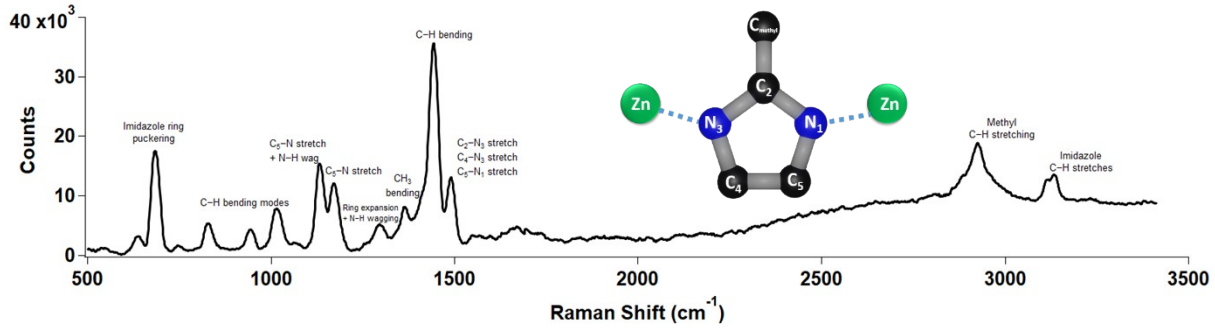

Figure S5: Raman spectra of ZIF-8 grown in the optical trap. Peaks identified by comparison to reported values.[5,6] Inset cartoon shows the organic linker, 2-Mim, bound to Zn^{2+} metal ions as would be found in the ZIF-8 crystal.

Plasmon Resonance Spectra

Spectra are analyzed in IgorPro using custom written code. A Gaussian curve is fit to the spectra in order to determine a peak wavelength and intensity. In part A of Figures S7-S10, the left plot in the raw spectra measurement, and the right is the Gaussian fits for that data. These figures

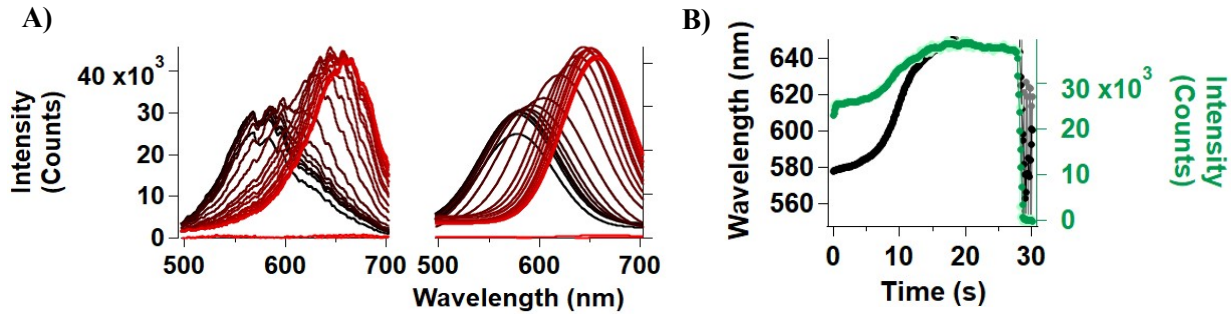

Figure S6: A) DF spectra collected following heating of an optically trapped, 80 nm AuNP in the presence of ZIF-8 precursors, 2-methylimidazole and $Zn(NO_3)_2$ in DMF **B)** Plot of the peak wavelengths (left, back) and associated intensities (right, green) against time.

demonstrate that growth is achieved in a variety of solvents. Spectra are collected sequentially at 10 Hz at 100 ms acquisition times over the spectral range of 496.184 nm – 702.815 nm.

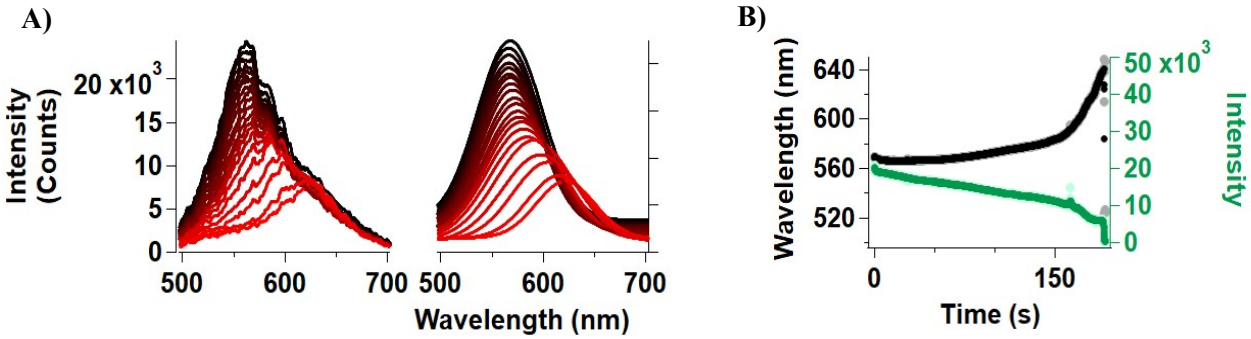

Figure S7: A) DF spectra collected following heating of an optically trapped, 80 nm AuNP in the presence of ZIF-8 precursors, 2-methylimidazole and $Zn(NO_3)_2$ in DMF exhibiting decreasing intensity. **B)** Plot of the peak wavelengths (left, back) and associated intensities (right, green) against time.

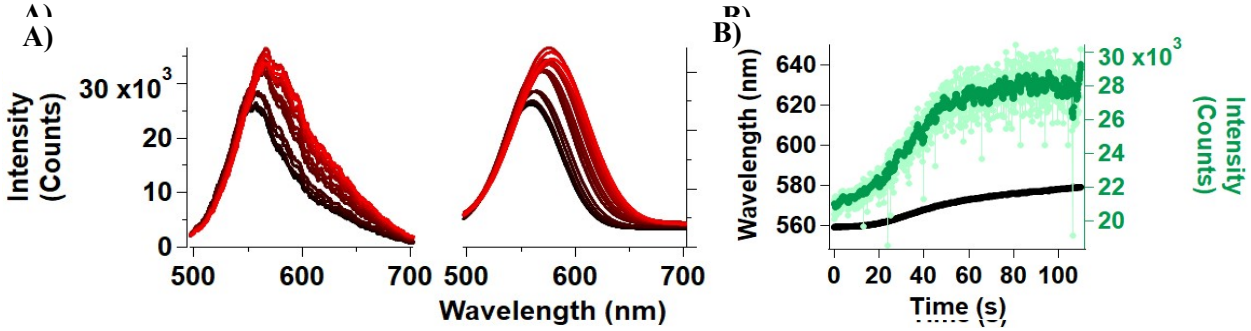

Figure S9: A) DF spectra collected following heating of an optically trapped, 80 nm AuNP in the presence of $Co(NO_3)_2$ and 4-tertbutylimidazole in water **B)** Plot of the peak wavelengths (left, back) and associated intensities (right, green) against time.

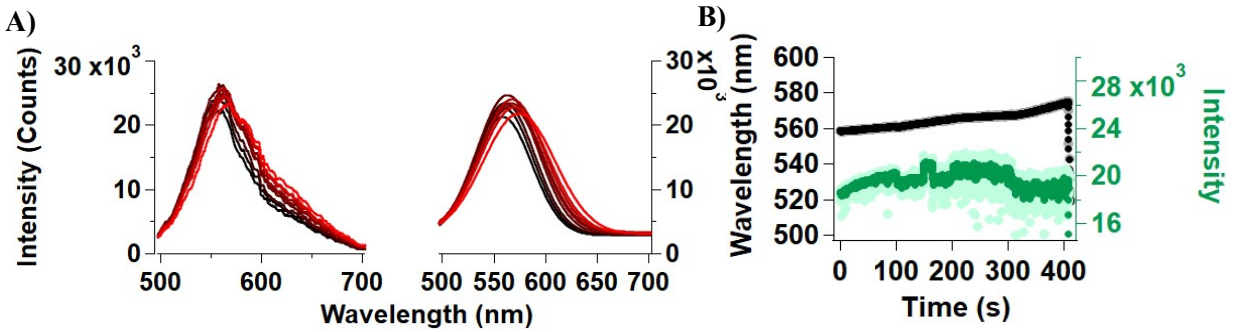

Figure S10: A) DF spectra collected following heating of an optically trapped, 80 nm AuNP in the presence of ZIF-67 precursors ($Co(NO_3)_2$ and 2-methylimidazole) in ethanol. **B)** Plot of the peak wavelengths (left, back) and associated intensities (right, green) against time.

Loss of Distinct Peak

Calculated the scattering cross sections of core@shell Au@ZIF particles using MATLAB package MNPBEM17.[7] As the shell thickness is increased, the scattering resonance peak is predicted to broaden and red-shift. For thin shells (<100 nm) there is a clear peak that fits well to a Gaussian. For intermediate thicknesses (>100 nm, <250 nm) the peak begins to broaden significantly and lose the distinct Gaussian peak profile. For the thickest shells (>250 nm) the resonance peak has significantly diminished and has almost completely disappeared in the higher index calculation shown in Figures S11A and S11B respectively. Figure S11C is a zoom in of

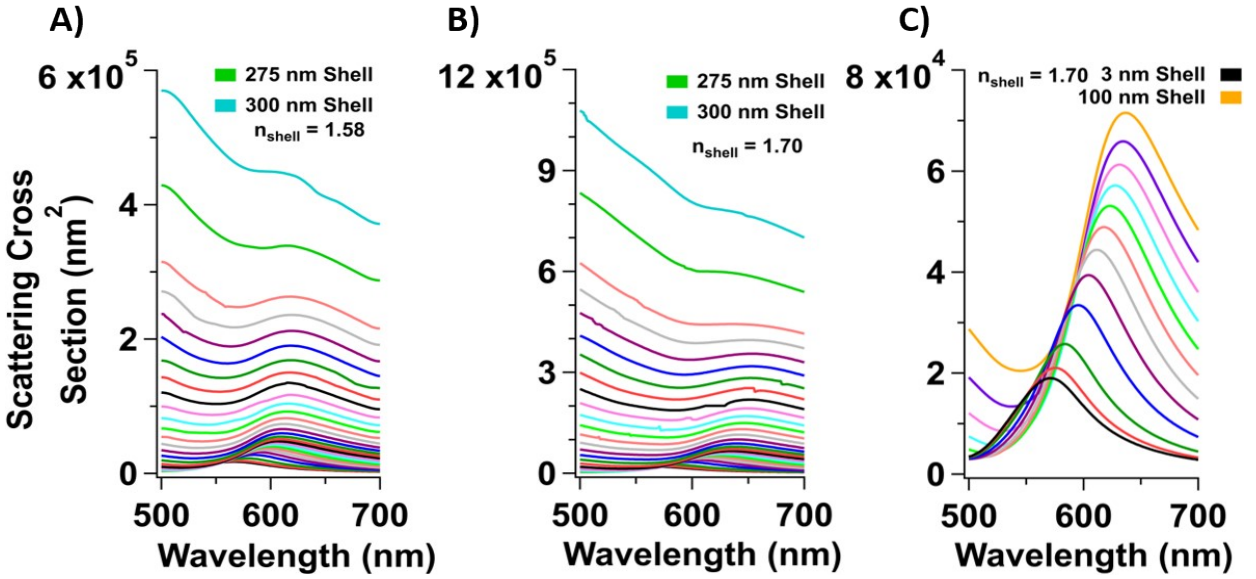

Figure S11: Model calculations of the scattering cross section of an 80 nm AuNP in ethanol for different thickness ZIF shells. **A)** Calculation shell with refractive index n=1.58 as listed by Cookney et al. **B)** Calculation shell with refractive index n=1.70 to agree with measured data. **C)** A zoom in of **B** to emphasize the difference in peak shape between thin shell scattering and thick shell scattering.

S9B on the thinnest shells to emphasize the difference in scattering profile between the thickest and thinnest shells we modelled.

Histograms of Crystal Growth

Final 3% of the data points for each particle prior to ejection from the trap is binned to determine an average final wavelength. Colors here match up to the colors used in the main manuscript: 2-Mim (green), 4-TBim (orange), Bim (purple), and 6-BBim (blue). Left plots the histogram for final wavelengths. The right is the histogram for final intensities. Solid curves are Gaussian fits to the histograms.

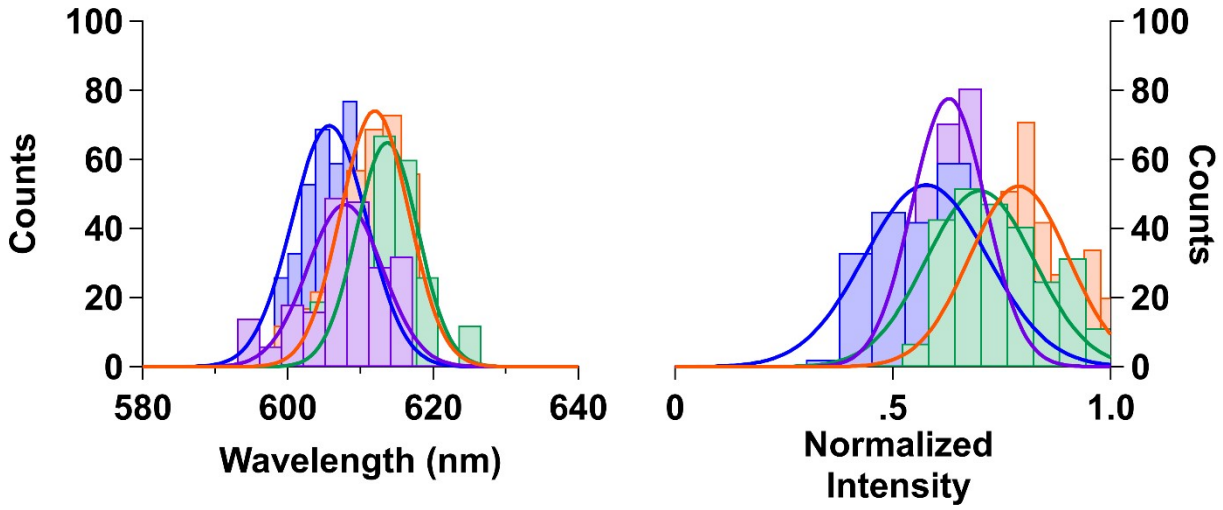

Figure S12: *left*) Histogram of the max wavelengths measured during growth. *right*) Histogram of the max intensities measured during growth

Heating of Gold Nanoparticles

We model the temperature near the surface of an optically trapped AuNP as previously reported.[8,9] The results are reproduced here in Figure S13. Briefly, we determine an absorption cross section for an 80 nm AuNP and calculate the local temperature as a function of distance from particle surface when it is placed in a uniform electro-magnetic field of varying intensities. The identity of the solvent, in particular its thermal conductivity, determines the temperature profiles and average temperatures around the particle, . Here, we model heating in ethanol to correspond to our experimental conditions.

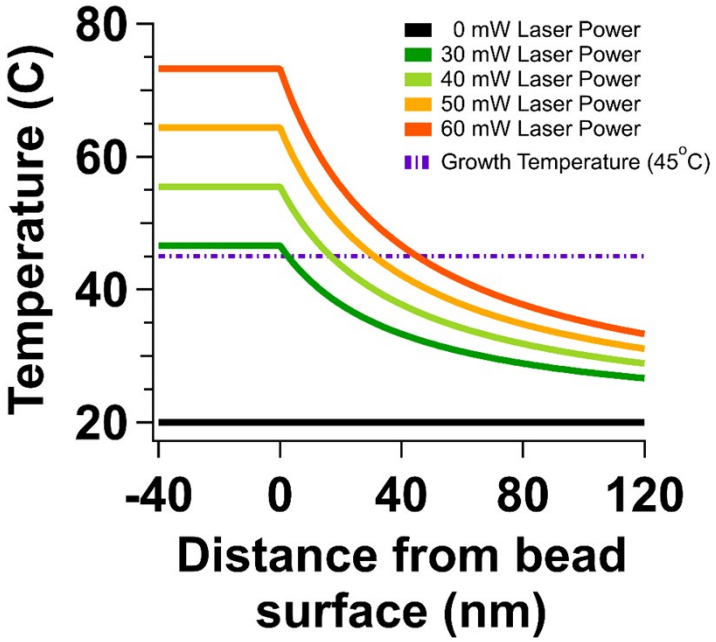

Figure S13: Showing the temperature decays for temperatures associated with powers used in figure 6 of main paper. Calculation for an 80 nm diameter AuNP in a sharply focused optical trap, located 200 nm above the focal plane in ethanol as the solvent.Black line represents room temperature, or a 0 mW trap. Purple dashed line is 45 ºC which we claim to be the cut-off temperature for driving growth with this technique

References

(1) Chen, L.; Peng, Y.; Wang, H.; Gu, Z.; Duan, C. Synthesis of Au@ZIF-8 Single- or Multi-Core–Shell Structures for Photocatalysis. *Chem. Commun.* **2014**, *50* (63), 8651–8654. https://doi.org/10.1039/C4CC02818J.

(2) Chen, Q. Q.; Hou, R. N.; Zhu, Y. Z.; Wang, X. T.; Zhang, H.; Zhang, Y. J.; Zhang, L.; Tian, Z. Q.; Li, J. F. Au@ZIF-8 Core-Shell Nanoparticles as a SERS Substrate for Volatile Organic Compound Gas Detection. *Anal. Chem.* **2021**, *93* (19), 7188–7195. https://doi.org/10.1021/ACS.ANALCHEM.0C05432/ASSET/IMAGES/LARGE/AC0C05432_0007.JPEG.

(3) Khan, I. U.; Othman, M. H. D.; Jilani, A.; Ismail, A. F.; Hashim, H.; Jaafar, J.; Rahman, M. A.; Rehman, G. U. Economical, Environmental Friendly Synthesis, Characterization for the Production of Zeolitic Imidazolate Framework-8 (ZIF-8) Nanoparticles with Enhanced CO2 Adsorption. *Arab. J. Chem.* **2018**, *11* (7), 1072–1083. https://doi.org/10.1016/J.ARABJC.2018.07.012.

(4) Park, K. S.; Ni, Z.; Cô, A. P.; Choi, J. Y.; Huang, R.; Uribe-Romo, F. J.; Chae, H. K.; O'keeffe, M.; Yaghi, O. M. Exceptional Chemical and Thermal Stability of Zeolitic Imidazolate Frameworks. *PNAS* **2006**, *103* (27), 10186–10191. https://doi.org/https://doi.org/10.1073/pnas.0602439103.

(5) Kumari, G.; Jayaramulu, K.; Maji, T. K.; Narayana, C. Temperature Induced Structural Transformations and Gas Adsorption in the Zeolitic Imidazolate Framework ZIF-8: A Raman Study. *J. Phys. Chem. A* **2013**, *117* (43), 11006–11012. https://doi.org/https://doi.org/10.1021/jp407792a.

(6) Gugin, N.; Jose Villajos, A.; Feldmann, I.; Emmerling, F.; Villajos, J. A.; Feldmann, I.; Emmerling, F. Mix and Wait – a Relaxed Way for Synthesizing ZIF-8. *RSC Adv.* **2022**, *12*, 8940–8944. https://doi.org/10.1039/d2ra00740a.

(7) Hohenester, U.; Trügler, A. MNPBEM – A Matlab Toolbox for the Simulation of Plasmonic Nanoparticles. *Comput. Phys. Commun.* **2012**, *183* (2), 370–381. https://doi.org/10.1016/J.CPC.2011.09.009.

(8) Jackson, D. J.; Dawes, B. A.; Kamenetska, M. Simultaneous Force and Darkfield Measurements Reveal Solvent-Dependent Axial Control of Optically Trapped Gold Nanoparticles. *J. Phys. Chem. Lett* **2023**, *14* (11), 2830–2836. https://doi.org/10.1021/acs.jpclett.3c00088.

(9) Seol, Y.; Carpenter, A. E.; Perkins, T. T. Gold Nanoparticles: Enhanced Optical Trapping and Sensitivity Coupled with Significant Heating. *Opt. Lett.* **2006**, *31* (16), 2429–2431. https://doi.org/10.1364/OL.31.002429.